ACS central science

Research Article

http://pubs.acs.org/journal/acscii

High-Potential Electrocatalytic O_2 Reduction with Nitroxyl/NO_x Mediators: Implications for Fuel Cells and Aerobic Oxidation Catalysis

James B. Gerken and Shannon S. Stahl*

Department of Chemistry, University of Wisconsin-Madison, 1101 University Avenue, Madison, Wisconsin 53706, United States

Supporting Information

ABSTRACT: Efficient reduction of O_2 to water is a central challenge in energy conversion and many aerobic oxidation reactions. Here, we show that the electrochemical oxygen reduction reaction (ORR) can be achieved at high potentials by using soluble organic nitroxyl and nitrogen oxide (NO_x) mediators. When used alone, neither organic nitroxyls, such as 2,2,6,6-tetramethyl-1-piperidinyl-*N*-oxyl (TEMPO), nor NO_x species, such as sodium nitrite, are effective ORR mediators. The combination of nitroxyl/NO_x species, however, mediates sustained O_2 reduction with overpotentials as low as 300 mV in acetonitrile containing trifluoroacetic acid. Mechanistic analysis of the coupled redox reactions supports a process in which the nitrogen oxide catalyst drives aerobic oxidation of a nitroxyl mediator to an oxoammonium species, which then is reduced back to the nitroxyl at the cathode. The electrolysis potential is dictated by the oxoammonium/nitroxyl reduction potential. The overpotentials accessible with this ORR system are significantly lower than widely studied molecular metal-macrocycle ORR catalysts and benefit from the mechanism-based specificity for four-electron reduction of oxygen to water mediated by NO_x species, together with kinetically efficient reduction of oxidized NO_x species by TEMPO and other organic nitroxyls.

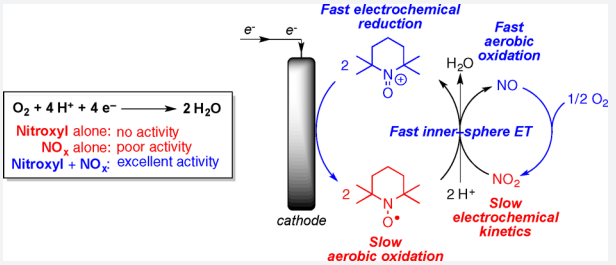

INTRODUCTION

Fuel cells operate via the coupling of two complementary half-reactions: (1) oxidation of a fuel, such as H_2, and (2) reduction of O_2 to water (Scheme 1A). Many catalytic aerobic oxidation reactions feature similar coupling of two half-reactions, whereby selective oxidation of an organic molecule ($SubH_2$) is mediated by the oxidized catalyst and O_2 is used to oxidize the reduced catalyst (Scheme 1B). In order for fuel cells to achieve the highest possible energy efficiency, the oxygen reduction reaction (ORR) must be kinetically facile at electrochemical potentials close to the thermodynamic potential for O_2 reduction. Formation of hydrogen peroxide as an intermediate or byproduct inherently limits the half-cell potential at the cathode (Table 1, eqs 1 and 2).[1] Molecular ORR catalysts, such as metalloporphyrins and related macrocyclic metal complexes, have been the focus of extensive investigation,[2,3] but such catalysts typically operate at

Scheme 1. Conceptual Similarity between Fuel Cells and Aerobic Oxidation Reactions

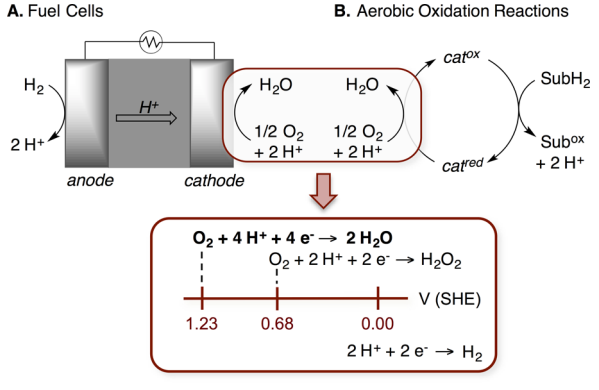

Table 1. Thermodynamic Values Associated with O_2 Reduction and NO_x-Based Redox Reactions in Aqueous Solution

eq	reaction	ΔG° or E°	refs
	O_2 Reduction Reactions		
1[a]	$O_2 + 4H^+ + 4e^- \rightleftharpoons 2H_2O$	1.23 V	12
2[a]	$O_2 + 2H^+ + 2e^- \rightleftharpoons H_2O_2$	0.68 V	12
	NO_x-Based Redox Reactions		
3[b]	$O_2 + 2NO^\bullet \rightleftharpoons 2NO_2$	−8.4 kcal·mol^{-1}	13
4[a]	$NO_2^\bullet + H^+ + e^- \rightleftharpoons 2HNO_2$	1.06 V	13, 14
5[a]	$HNO_2 + H^+ + e^- \rightleftharpoons H_2O + NO^\bullet$	1.04 V	13

[a]Aqueous solution, 1 atm. [b]Gas phase value.

Received: May 7, 2015
Published: July 15, 2015

DOI: 10.1021/acscentsci.5b00163
ACS Cent. Sci. 2015, 1, 234−243

potentials far from the thermodynamic limit and often generate hydrogen peroxide.[3d,4−8] Aerobic oxidation reactions of the type depicted in Scheme 1B face similar issues.[9] These catalytic reactions commonly proceed via two-electron redox cycles in which the O_2 reduction step produces hydrogen peroxide, which either accumulates[10] or undergoes disproportionation into O_2 and water.[11] The formation of H_2O_2 limits the driving force available to carry out the substrate oxidation half-reaction and thereby contributes to the widespread use of more expensive, toxic, or otherwise less desirable stoichiometric oxidants in challenging synthetic oxidation reactions.

Use of nitrogen oxide (NO_x) cocatalysts provides a potential opportunity to overcome the limitations noted above. The reaction of nitric oxide (NO) with oxygen is kinetically facile and thermodynamically favorable, and it results in direct cleavage of the O−O bond of O_2 to afford nitrogen dioxide (NO_2) without forming H_2O_2 as an intermediate or byproduct (Table 1, eq 3).[15] Moreover, the proton-coupled steps for reduction of NO_2 to NO exhibit standard potentials close to the thermodynamic potential for O_2 reduction to water (Table 1, eqs 4 and 5). The use of NO_x-based mediators to achieve high-potential ORR, however, is limited by poor direct electrochemical reduction of NO_x species.[16,17] Previous efforts to overcome this limitation have used NO_x species in combination with the VO^{2+}/VO_2^+ couple to achieve electrocatalytic O_2 reduction.[18] However, vanadyl is similarly problematic as a mediator due to its own slow heterogeneous electron-transfer kinetics, probably arising from the large inner-sphere reorganization associated with VO_2^+ reduction.[19] An ideal mediator would exhibit facile kinetics at the electrode, in addition to undergoing rapid reaction with NO_x species derived from O_2 reduction.

The above considerations drew our attention to catalytic aerobic alcohol oxidation reactions that employ 2,2,6,6-tetramethylpiperidinyl-*N*-oxyl (TEMPO) or other organic nitroxyls in combination with NO_x-based cocatalysts (Scheme 2A).[20,21] We speculated that the alcohol substrate could be replaced with an electrode (Scheme 2B) to provide the basis for nitroxyl/NO_x-mediated electrocatalytic O_2 reduction. The results presented below validate this concept and show that the nitroxyl/NO_x cocatalysts enable O_2 reduction at overpotentials at least 200 mV lower than those previously attained with molecular ORR electrocatalysts. Mechanistic studies provide key insights into the nitroxyl and NO_x redox reactions and have important implications for both ORR electrocatalysis and aerobic oxidation of organic molecules.

Scheme 2. Catalytic Cycles for TEMPO/NO_x-Mediated Aerobic Alcohol Oxidation (A) and Electrocatalytic O_2 Reduction (B)

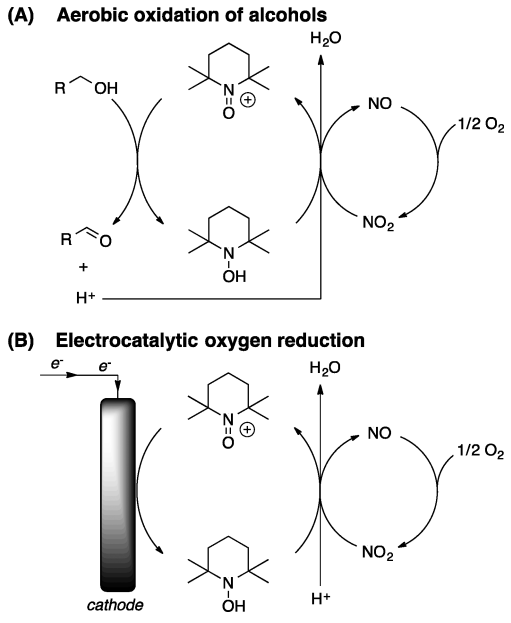

RESULTS AND DISCUSSION

Nitroxyl Disproportionation by Acid and Oxidation by $NaNO_2$. TEMPO is an organic radical that is stable in organic and neutral aqueous solutions for extended periods. Under acidic conditions, however, TEMPO undergoes disproportionation to the corresponding oxoammonium and hydroxylamine species eq 6.[22] This reactivity was probed in acetonitrile under acidic

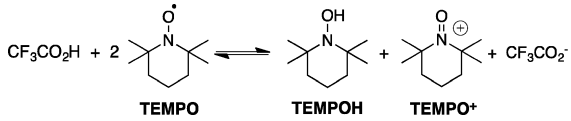

(6)

conditions similar to those used in TEMPO/NO_x-catalyzed aerobic oxidation reactions. UV−visible spectra of TEMPO and independently generated oxoammonium and hydroxylamine species in acetonitrile are shown in Figure 1A. TEMPO exhibits a broad absorption band, with a maximum at 459 nm. The TEMPO-derived oxoammonium species, $TEMPO^+$, exhibits an absorption maximum in a similar region (λ_{max} = 473 nm, ε_{max} = 20.3 $M^{-1}\cdot cm^{-1}$), but has an extinction coefficient approximately twice that of TEMPO ($\varepsilon_{459\text{-TEMPO}}$ = 10.5 $M^{-1}\cdot cm^{-1}$; $\varepsilon_{459\text{-TEMPO+}}$ = 20.0 $M^{-1}\cdot cm^{-1}$). The hydroxylamine species, TEMPOH, has negligible absorbance in this region.

Addition of excess trifluoroacetic acid (TFAH, 13 equiv) to a solution of TEMPO (10 mM) in acetonitrile results in spectral changes consistent with the conversion of TEMPO to $TEMPO^+$ and TEMPOH (Figure 1B; cf. eq 6). The change in nitroxyl concentration over time was obtained by curve-fitting, using the known spectra for TEMPO and $TEMPO^+$,[24] and the kinetic data exhibit a second-order dependence on [TEMPO], with a k_{obs} of 2.5 M^{-1} s^{-1} (see inset, Figure 1B). The system reaches equilibrium with significant disproportionation ($K_{eq} \approx 0.4$ for eq 6, corresponding to $[TEMPO^+]/[TEMPO] = 3.5$). The resulting solution exhibits negligible changes upon standing in air for 30−40 min, indicating that TEMPOH formed upon TEMPO disproportionation does not undergo facile oxidation by dissolved O_2.

The reactivity of TEMPO-derived disproportionation species with $NaNO_2$ was then investigated under anaerobic conditions. Addition of a substoichiometric quantity of $NaNO_2$ (0.09 equiv) led to a growth of the $TEMPO^+$ spectral feature. The amount of $TEMPO^+$ formed via oxidation of TEMPOH is consistent with nitrite serving as a one-electron oxidant (Figure 1C and eq 7).

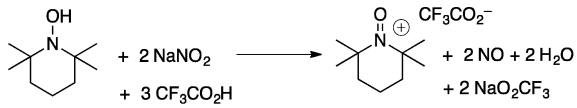

(7)

Subsequent addition of excess $NaNO_2$ (1.4 equiv relative to the original [TEMPO]) results in complete conversion to $TEMPO^+$. The spectrum of the fully oxidized TEMPO solution is very close to that of a doubled spectrum of the TEMPO disproportionation solution before addition of $NaNO_2$, which contained a nearly

DOI: 10.1021/acscentsci.5b00163
ACS Cent. Sci. 2015, 1, 234−243

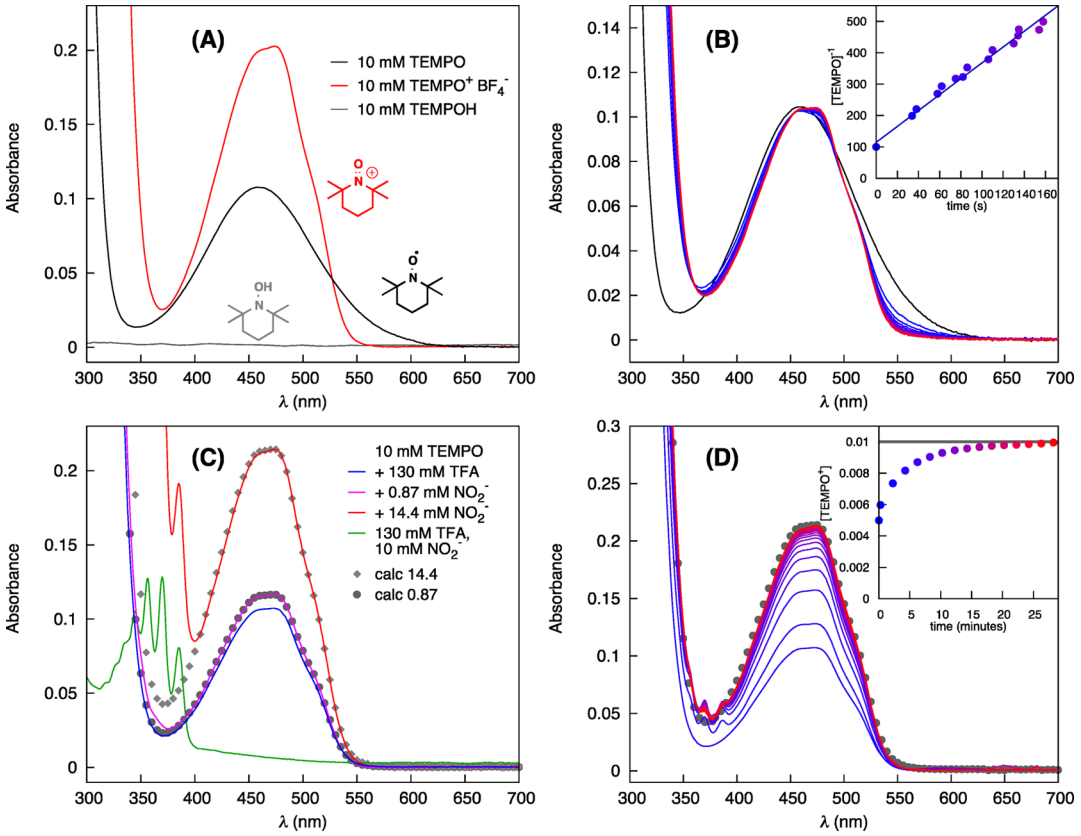

Figure 1. UV−visible studies of TEMPO disproportionation and reactivity with $NaNO_2$ under acidic conditions in acetonitrile. (A) Spectra of 10 mM $TEMPO^+$, TEMPO, and TEMPOH in CH_3CN.[23] (B) Spectra obtained following addition of trifluoroacetic acid (TFAH) to a 10 mM solution of TEMPO, corresponding to TEMPO disproportionation into $TEMPO^+$ and TEMPOH eq 6. The linear fit to $[TEMPO]^{-1}$ (inset) incorporates data from three independent experiments. Conditions: 10 mM TEMPO in CH_3CN, 130 mM TFA added at $t = 0$. (C) Spectral changes observed upon addition of $NaNO_2$ (0.09 and 1.4 equiv) to a disproportionated-TEMPO solution in CH_3CN/TFAH under N_2. The changes reflect oxidation of TEMPOH to $TEMPO^+$ by nitrite. The gray points represent the expected spectrum for full conversion of NO_2^- to NO or TEMPO to $TEMPO^+$ depending on the limiting reagent. Conditions: 10 mM TEMPO in CH_3CN with 130 mM TFA, 0.9 or 14.4 mM $NaNO_2$, N_2 atmosphere. (D) Aerobic oxidation of disproportionated TEMPO catalyzed by nitrite. The initial spectrum of $TEMPO^+$ with colorless TEMPOH shifts to higher absorbance as more $TEMPO^+$ is formed (blue → red, 2 min scan interval). The gray dotted spectrum depicts the spectrum expected if all TEMPO-based species are converted to $TEMPO^+$. Conditions: 10 mM TEMPO in CH_3CN with 130 mM TFA, 0.9 mM $NaNO_2$ added at $t = 0$, 1 atm O_2.

50:50 mixture of $TEMPO^+$ and TEMPOH. These results show that nitrite is an effective oxidant for the conversion of TEMPOH to $TEMPO^+$.

Nitrite can undergo disproportionation into NO_2 and NO under acidic conditions eq 8,[16] and NO_2 is believed to be the active oxidant under these conditions. A spectrum of nitrite in the presence of acid shows a series of peaks with λ_{max} of 345, 356, 370, and 385 nm (green trace, Figure 1C), which are in good agreement with a species previously assigned to HNO_2.[25,26] The latter species is a precursor to the NO_2 oxidant (see further discussion below).

$$2NaNO_2 + 2CF_3CO_2H \rightleftharpoons NO_2 + NO + H_2O + 2CF_3CO_2Na \quad (8)$$

Addition of substoichiometric nitrite (0.09 equiv) to the TEMPO-disproportionation solution under *aerobic* conditions (1 atm O_2) leads to complete conversion to $TEMPO^+$ within 30 min (Figure 1D). As the experiments described above showed that TEMPOH undergoes negligible direct oxidation by O_2, this process is attributed to NO_x-catalyzed aerobic oxidation of TEMPOH, resembling the process invoked in aerobic alcohol oxidation reactions (cf. Scheme 2A). Again, the peaks between 350 and 400 nm that grow in and decrease during the catalytic oxidation are consistent with the presence of dissolved HNO_2, possibly with some N_2O_4.[27]

Electrochemical Studies of TEMPO and TEMPO/NO_x Solutions. Cyclic voltammetry (CV) measurements of TEMPO in CH_3CN show the expected reversible nitroxyl/oxoammonium redox process at $E_{1/2}$ = 249 mV vs ferrocene/ferrocenium (Fc/Fc^+; see Figure 2, black trace).[28] Addition of 130 mM trifluoroacetic acid to the CH_3CN solution induces disproportionation of TEMPO into the oxoammonium and hydroxylamine species, as described above (eq 6, Figure 1B). This process is manifested by an increase in the open-circuit potential of the solution that reflects formation of the oxoammonium species $TEMPO^+$. TEMPO disproportionation is relatively slow on the CV time scale, as revealed by two features in the red trace of Figure 2. First, a broad irreversible peak corresponding to proton-coupled reduction of TEMPO to TEMPOH is evident at low potential (ca. −0.32 V in Figure 2). The availability of TEMPO to participate in this process indicates that TEMPO formed via reduction of the $TEMPO^+$ has not undergone disproportionation into $TEMPO^+$/TEMPOH on the time scale of the scan. Second, a CV peak associated with oxidation of TEMPO to $TEMPO^+$ in the reverse anodic scan provides support for the persistence of TEMPO on the CV time scale.

DOI: 10.1021/acscentsci.5b00163
ACS Cent. Sci. 2015, 1, 234−243

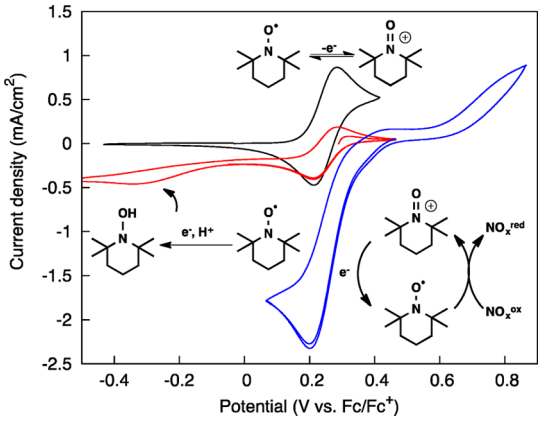

Figure 2. Cyclic voltammograms of TEMPO under anaerobic conditions in CH_3CN (black trace) and following sequential addition of CF_3CO_2H (130 mM, red trace) and $NaNO_2$ (2 equiv, blue trace), also under anaerobic conditions. Standard conditions: 10 mM TEMPO, 0.5 M KPF_6, N_2 atmosphere, scan rate = 10 mV/s, glassy carbon electrode.

Addition of $NaNO_2$ (2 equiv relative to TEMPO) to the solution under anaerobic conditions leads to complete oxidation of TEMPO to the oxoammonium species, as revealed by the lack of a CV feature associated with oxidation of the nitroxyl in the anodic scan (Figure 2, blue trace). A catalytic wave, evident at the $TEMPO^+$/TEMPO potential in the cathodic scan, is attributed to TEMPO-catalyzed reduction of excess nitrite, HNO_2, or other oxidized NO_x species present in solution.[29] An irreversible anodic feature at $E_p \approx 0.80$ V is assigned to oxidation of dissolved NO produced from nitrite reduction (or disproportionation) in the absence of O_2 (cf. Table 1, eq 5).[30]

A catalytic CV wave very similar to the blue trace in Figure 2 is observed when the same experiment is performed under aerobic conditions. In order to better assess the ability of NO_x to serve as a catalytic mediator for electrochemical O_2 reduction, controlled potential electrolysis studies were performed under aerobic conditions with the electrode potential set at 0.20 V vs Fc/Fc^+. The combination of TEMPO and $NaNO_2$ produces significant sustained catalytic current (Figure 3, red trace). The amount of charge passed during the 2 h electrolysis corresponds to a TEMPO-based turnover number of 93 and a turnover frequency

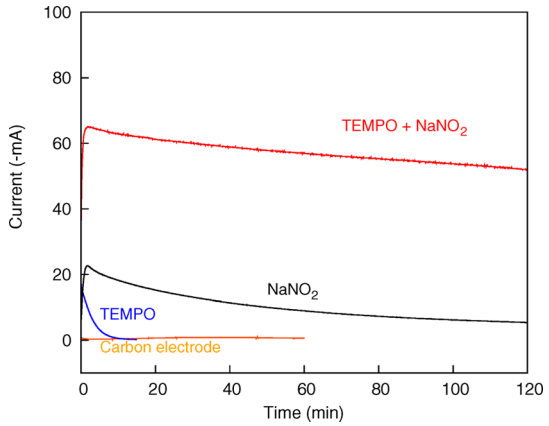

Figure 3. Controlled-potential electrolysis traces with and without $TEMPO/NO_x$ mediators at 0.20 V vs Fc/Fc^+ in 9:1 CH_3CN:CF_3CO_2H under 1 atm O_2. Conditions: 0.5 M KPF_6 + 1.25 mM $NaNO_2$, 1.25 mM TEMPO, 1.25 mM $NaNO_2$ + 1.25 mM TEMPO, or no added catalyst/mediator.

of 46 e^-/h.[31] The slow decrease in the electrolysis current is attributed to a steady loss of active NO_x species from the stirred solution into the gas phase.[32] A control experiment demonstrated that the carbon electrode does not mediate catalytic oxygen reduction in the absence of $NaNO_2$ (Figure 3, orange trace). A solution of TEMPO alone reveals only a small electrolysis current that decays rapidly (Figure 3, blue trace), corresponding to stoichiometric reduction of $TEMPO^+$ generated from TEMPO disproportionation. A low level of catalytic activity is evident from a solution of $NaNO_2$ in the absence of TEMPO (Figure 3, black trace), but the current decays to near-zero during the 2 h electrolysis. Collectively, these data demonstrate that both TEMPO and NO_x species are important for electrocatalytic ORR activity.

Scheme 3. Structures of 4-AcetamidoTEMPO (ACT), 3-CarbamoylPROXYL (3-CARP), and ABNO

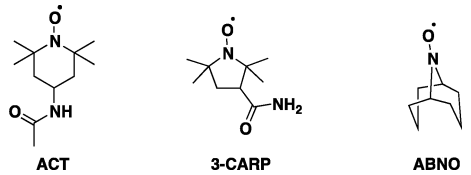

Electrocatalytic O_2 Reduction with Other Nitroxyl/NO_x Combinations. The successful electrocatalytic ORR results with $TEMPO/NO_x$ prompted us to examine three other organic nitroxyl mediators (Scheme 3): 4-acetamidoTEMPO (ACT), 3-carbamoyl-2,2,5,5-tetramethyl-1-pyrrolidinyl-N-oxyl (3-carbamoylPROXYL or 3-CARP), and 9-azabicyclo[3.3.1]nonane-*N*-oxyl (ABNO). The ACT and 3-CARP oxoammonium/nitroxyl redox potentials ($E_{1/2}$ = 324 and 346 mV, respectively) are 75 and 97 mV higher than TEMPO ($E_{1/2}$ = 249 mV), while the ABNO potential ($E_{1/2}$ = 229 mV) is similar to that of TEMPO (Figure 4). UV–visible studies show that ACT and 3-CARP disproportionate at a slower rate and to a smaller degree relative to TEMPO (see Supporting Information for details),[33] and CVs of these nitroxyls under acidic conditions (red traces, Figure 4) are consistent with slow disproportionation on the CV time scale, similar to that of TEMPO described above. ABNO is unique relative to the other three nitroxyls, as it undergoes rapid disproportionation on the CV time scale (Figure 4).[34] There is no peak for reduction of the nitroxyl to hydroxylamine at low potentials because reduction of $ABNO^+$ to ABNO combines with ABNO disproportionation to afford ABNOH at the $ABNO^+$/ABNO reduction potential. The peak cathodic current for ABNO in acid is similar to the anodic current without acid, showing that the oxoammonium formed by disproportionation must be undergoing a net 2-electron reduction at the $ABNO^+$/ABNO potential. The irreversibility of the reduction of ABNO in acid, evident from the lack of a peak in the anodic scan, also implies that the ultimate reduction product is the hydroxylamine.

Each of these three nitroxyls proved to be effective mediators of O_2 reduction under controlled potential electrolysis conditions at 0.32, 0.33, and 0.19 V, respectively, for ACT, 3-CARP, and ABNO (Figure 5). ACT and 3-CARP show very similar catalytic performance, as might be expected from their similar redox properties. ABNO exhibits higher steady-state catalytic current than TEMPO, even though these nitroxyls have nearly identical $E_{1/2}$ values. The higher currents observed with ABNO may be related to its more-facile disproportionation or oxidation (cf. Figures S10 and S11), although a full mechanistic

DOI: 10.1021/acscentsci.5b00163
ACS Cent. Sci. 2015, 1, 234–243

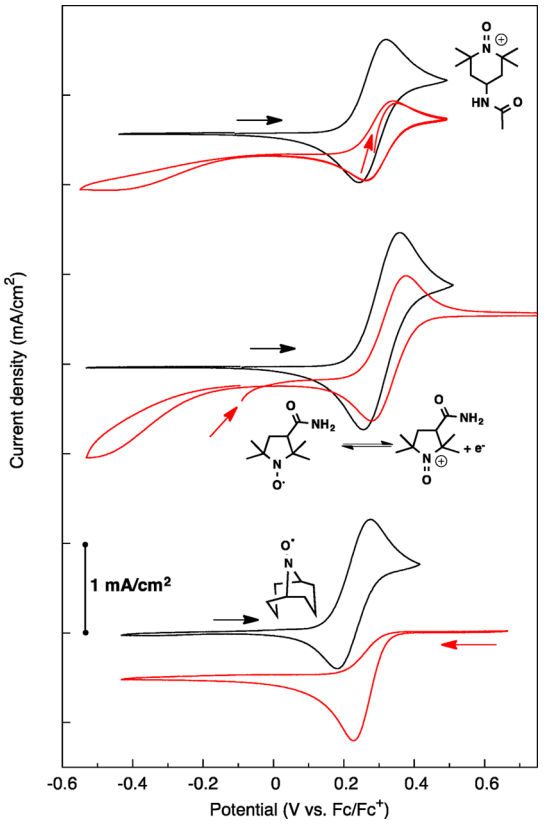

Figure 4. Cyclic voltammograms of ACT, 3-CARP, and ABNO under anaerobic conditions in CH_3CN (black trace) and following addition of CF_3CO_2H (130 mM, red trace). Standard conditions: 10 mM nitroxyl, 0.1 M KPF_6, N_2 atmosphere, scan rate = 10 mV/s, glassy carbon electrode. Arrows indicate the starting potential of each scan.

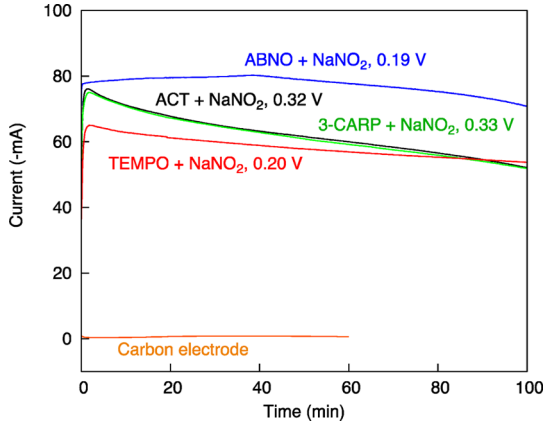

Figure 5. Controlled-potential electrolysis traces with ACT (black), 3-CARP (green), and ABNO (blue) mediators in combination with $NaNO_2$ as a NO_x source at 0.32, 0.33, and 0.19 V, respectively, vs Fc/Fc^+ in 9:1 CH_3CN:CF_3CO_2H under 1 atm O_2. The TEMPO (red) trace is reproduced from Figure 3 for comparison. Conditions: 0.5 M KPF_6 + 1.25 mM $NaNO_2$, 1.25 mM nitroxyl.

rationale will require further investigation. Most significantly, these results demonstrate that the operating potential for O_2 reduction is established by the reduction potential of the oxoammonium species present. This result is noteworthy because the pH-independent reduction potentials of the four nitroxyls studied here (0.23−0.35 V vs Fc/Fc^+ or 0.87−0.99 V vs NHE) are significantly higher than redox potentials of previously studied molecular ORR catalysts (see below for an estimate of the overpotential and further discussion).

Analysis of the Catalytic Mechanism. The above data highlight the ability to achieve high-potential electrocatalytic O_2 reduction by using an appropriate combination of electron- and/or electron/proton-transfer mediators.[35] The synergy between the nitroxyl and NO_x cocatalysts is evident from the inability of the individual components to mediate independent ORR electrocatalysis. NO_x species undergo rapid reaction with O_2 but react slowly at the electrode, while nitroxyls exhibit good electrode reactivity but react poorly with O_2. The facile reactivity of the nitroxyl and NO_x species with each other enables the positive traits of the nitroxyl/NO_x partners to achieve efficient electrocatalytic O_2 reduction.

Insights into the unique properties of the nitroxyl/NO_x cocatalyst combination can be gleaned from the data above as well as previous literature,[36−40] and the tandem catalytic cycle in Scheme 4 provides the basis for our analysis. At the electrode,

Scheme 4. Proposed Mechanism for the TEMPO-Mediated Electrocatalytic Reduction of O_2 by NO_x[a]

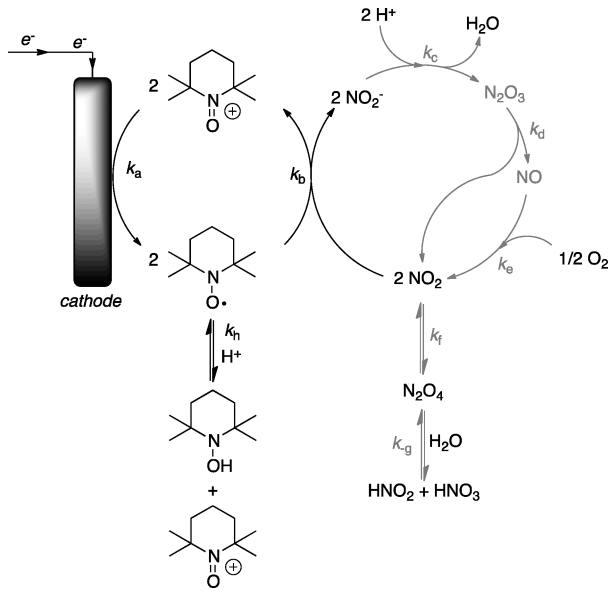

[a]Species and processes for which there is evidence from the present work are in black, ones inferred from the literature are in gray (see below).

$TEMPO^+$ is reduced to TEMPO radical, which may be reoxidized by NO_2 to close the left-hand cycle. TEMPO disproportionation appears to be relatively slow under the reaction conditions and therefore is proposed to be off-cycle. Nevertheless, oxidation of TEMPOH by NO_2 is facile and provides another entry into the catalytic cycle (cf. Figure 1D). The reduction of NO_2 by TEMPO generates nitrite, which undergoes protonation and release of water in a sequence of steps that eventually forms NO.[16] Aerobic oxidation of NO to NO_2 is facile[15] and closes the right-hand cycle of the catalytic mechanism. Rapid reaction of TEMPO with NO_2 minimizes the conversion of NO_2 into HNO_3 in an undesirable off-cycle pathway.[41]

Nitrogen oxide species (NO_x) have been the subject of intense study, *inter alia*, as catalysts, as atmospheric pollutants, and for their role in biology,[16,42,43] and kinetic and thermodynamic data for various NO_x- and TEMPO-based reactions obtained from

DOI: 10.1021/acscentsci.5b00163
ACS Cent. Sci. 2015, 1, 234−243

those studies support the mechanism in Scheme 4 (see Table S1 and associated text for details).

The other nitroxyls used in this study are expected to react via the same mechanism as TEMPO, and ACT, 3-CARP, and ABNO display similar steady-state catalytic currents when the electrolysis potential is adjusted to account for the different $E_{1/2}$ values. In principle, the electrode potential could be increased further by using nitroxyls with even higher $E_{1/2}$ values as long as the reduction potential of NO_2 is high relative to that of the nitroxyl. As the oxoammonium reduction potential increases, its oxidation by NO_2 becomes less favorable.[36a] The resulting increase in the steady state concentration of NO_2 may be the source of the more rapidly decreasing current observed with ACT and 3-CARP, relative to TEMPO and ABNO (Figure 5), owing to the competing conversion of NO_2 into HNO_3.

Estimate of Overpotential and Comparison of Nitroxyl/NO_x with Other Molecular ORR Catalysts. Among the many molecular electrocatalysts that have been considered for O_2 reduction,[2−8,44] macrocyclic metal complexes, such as Fe and Co porphyrins and corroles, are among the most common. Other examples include Cu-oxidase and Fe/Cu-cytochrome *c* oxidase mimics.[44f,g] Strategic catalyst designs, including complexes with enforced proximity of two metal centers[2c,d,44a,b,e,f] or those that incorporate proton relays,[3c,5] have enabled good reaction rates to be achieved with good selectivity for H_2O over H_2O_2 as the reduction product (see Table S2 for structures, H_2O/H_2O_2 selectivities, and estimated overpotentials for over two dozen representative examples). Nevertheless, these catalysts typically operate at potentials where at least one metal ion is divalent (i.e., some bimetallic complexes may initiate the reaction from an M^{II}-M^{III} state) because complexes containing isolated trivalent metal centers typically exhibit little-to-no affinity for O_2 and are unable to initiate O_2 reduction (Scheme 5). In this context, fundamental

Scheme 5. Macrocyclic Metal Catalysts Initiate O_2 Binding and Reduction from the M^{II} Oxidation State (M = Fe, Co)

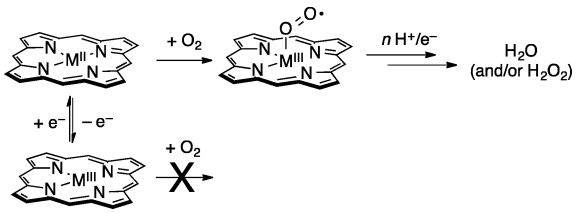

studies of cobalt porphyrins show that the $Co^{III/II}$ potential is inversely correlated with O_2 binding affinity of Co^{II}.[45] These considerations indicate that the ORR potential of metal-based catalysts will be pinned to the metal redox potential.[46] The highest ORR potentials have been observed with Co-based macrocycles, but, in spite of decades of research with such complexes, the electrode potentials observed for electrocatalytic O_2 reduction have not exceeded the $Co^{III/II}$ potential of cobalt tetraphenylporphyrin (CoTPP) by more than 200 mV. To our knowledge, the highest potentials have been observed with cofacial bis-[Co-porphyrin][44b] and Co-porphyrin/Co-corrole[47] conjugates, which operate at overpotentials of $\eta \approx 520$ mV (cf. Table S2).

It is not straightforward to assign overpotentials to the ORR reactions studied here due to uncertainties in the thermodynamic potential for O_2 reduction under the unbuffered nonaqueous reaction conditions.[48] According to the above discussion, however, the $Co^{III/II}$ potential for CoTPP serves as a useful benchmark, and the ORR activity observed with the ACT/NO_x and 3-CARP/NO_x takes place at a potentials nearly 500 mV higher than the $Co^{III/II}$ potential for CoTPP under the same conditions.[49]

It is also possible to estimate the thermodynamic potential of O_2 reduction as being 1.23 V above the H^+/H_2 potential under the same conditions. Therefore, the H^+/H_2 potential was measured in acetonitrile with a TFAH/NaTFA electrolyte (1 M each) according to a recently reported protocol.[50,51] The observed H^+/H_2 potential of −0.61 V vs Fc/Fc^+ (see Figure S14) corresponds to an O_2 reduction potential of +0.62 V. A steady-state ORR electrolysis experiment was then performed with the ACT/NO_x-mediator system under these conditions at an applied potential of +0.32 V vs Fc/Fc^+. The current was somewhat lower than that observed under the unbuffered conditions described above; however, >26 turnovers with respect to ACT were observed over a 4 h period. These results reflect catalytic ORR performance at an overpotential of only 300 mV.

This favorable performance is consistent with the high standard potentials associated with proton-coupled reduction of NO_2 (1.06 V vs NHE; cf. Equation 4 in Table 1) and reduction of ACT- and 3-CARP-derived oxoammonium species (0.96 and 0.99 V vs NHE, respectively). Nitric oxide is the NO_x species that binds O_2, and it may be generated at reduction potentials where metal-based catalysts are typically in an oxidation state incapable of binding O_2 and unreactive toward ORR.[52] Moreover, NO reacts rapidly with O_2 to form NO_2 with cleavage of the O−O bond, exhibiting specificity for the four-electron reduction of O_2.

Implications of NO_x/O_2 Reactivity for Aerobic Oxidation Reactions. The strategy employed here for high-potential electrocatalytic O_2 reduction was inspired by nitroxyl/NO_x-catalyzed aerobic alcohol oxidation (cf. Scheme 2). The electrocatalysis results also have implications for aerobic oxidation reactions, and they shed light on the growing interest in NO_x-based cocatalysts for aerobic oxidations, including reactions normally incompatible with O_2 as the oxidant. 2,3-Dichloro-5,6-dicyano-1,4-benzoquinone (DDQ) is a high-potential quinone that finds widespread use in organic chemical synthesis, but it is almost exclusively used as a stoichiometric reagent. Recent studies show, however, that NO_x-based cocatalysts may be used with *catalytic* DDQ in aerobic oxidation reactions, including dehydrogenation of saturated C−C bonds, oxidation of benzylic and allylic alcohols, oxidative cleavage of benzylic ethers, and oxidative C−C coupling reactions.[53]

Pd-catalyzed oxidation reactions involving high-valent (Pd^{III} or Pd^{IV}) intermediates typically require strong stoichiometric oxidants, such as hypervalent iodine reagents or electrophilic halogen sources.[54] While aerobic oxidation of Pd^0 is a key feature in many Pd^{II}/Pd^0-catalyzed oxidation reactions,[9a,55] the analogous oxidation of Pd^{II} to Pd^{IV} (or Pd^{III}) by O_2 is rare.[56] Several recent studies, however, show that NO_x cocatalysts enable efficient aerobic oxidation in reactions that probably proceed via high-valent Pd intermediates, such as the acetoxylation of benzene and vicinal dioxygenation of alkenes (Scheme 6A).[57] Many mechanistic features remain to be elucidated for these reactions, but NO_2 is proposed to oxidize organopalladium(II) species to high-valent Pd intermediates that undergo carbon-heteroatom bond formation (e.g., Scheme 6B). The effectiveness of NO_x cocatalysts undoubtedly reflects the increased driving force available from the one- or two-electron reductions of NO_2 to HNO_2 or NO/H_2O (cf. Table 1) relative to the analogous one- or two-electron reductions of O_2 to HO_2 or H_2O_2. Overall, these observations demonstrate that oxidation of NO to NO_2

DOI: 10.1021/acscentsci.5b00163
ACS Cent. Sci. 2015, 1, 234−243

Scheme 6. Catalytic Reactions and Possible Mechanism for the Role of NO_x Co-Catalysts in Catalytic Aerobic Oxidation Reactions that Proceed via High-Valent Pd Intermediates

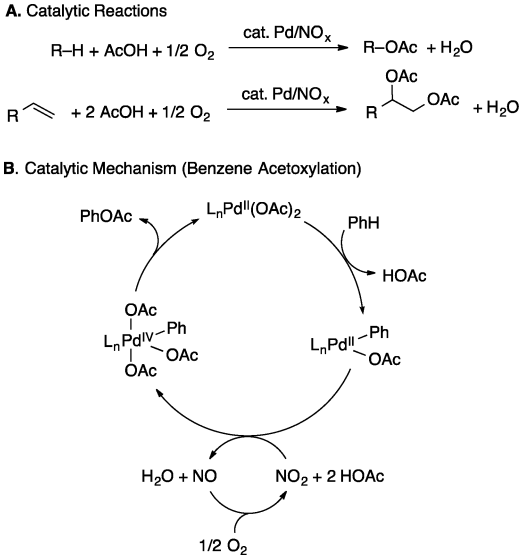

captures much of the free energy available from O_2 as an oxidant, and NO_2 is then capable of serving as an effective, kinetically advantageous high-potential oxidant.

CONCLUSION

This study demonstrates that by combining the facile electrochemistry of nitroxyls with the high-potential O_2 activation chemistry of NO_x, it is possible to achieve efficient electrocatalytic O_2 reduction at high potentials. The operating potential of the catalyst system is set by the reduction potential of the oxoammonium form of the nitroxyl mediator, while the catalyst stability is determined by the rate of decomposition of NO_x into unreactive species. The nitroxyl mediator helps to stabilize the catalyst by shifting the NO_x speciation toward intermediates that are less susceptible to decomposition. Organic nitroxyls alone do not reduce oxygen and NO_x alone displays sluggish electrochemistry, but together they create an efficient system that delivers much of the thermodynamic potential available from the four-electron reduction of O_2.

ASSOCIATED CONTENT

Supporting Information

The Supporting Information is available free of charge on the ACS Publications website at DOI: 10.1021/acscentsci.5b00163.

Experimental procedures, additional data and discussion, and worked examples of self-exchange rate and electrode-exchange current conversions. Additional content includes a tabulation of (1) literature rate constants of nitroxyl and NOx reactions and (2) data for previously reported molecular ORR catalysts and their overpotentials (PDF).

AUTHOR INFORMATION

Corresponding Author

*E-mail: stahl@chem.wisc.edu.

Notes

The authors declare the following competing financial interest(s): A patent has been filed on the basis of this work.

ACKNOWLEDGMENTS

We thank Tracy Drier for fabrication of the electrolysis cell, Yutong Pang for assistance with CV data collection, Dr. Alireza Rahimi for providing a sample of $ACT^+BF_4^-$, and Prof. James M. Mayer (Yale) for insightful critical feedback. We also thank a reviewer for suggesting measurement of the H^+/H_2 potential as a means to estimate the ORR overpotential for this system. This research was supported as part of the Center for Molecular Electrocatalysis, an Energy Frontier Research Center, funded by the U.S. Department of Energy, Office of Science, Office of Basic Energy Sciences.

REFERENCES

(1) Traditional ORR catalysts consist of platinum dispersed in a conductive carbon support. For leading references, see: (a) Gasteiger, H. A.; Kocha, S. S.; Sompalli, B.; Wagner, F. T. Activity benchmarks and requirements for Pt, Pt-alloy, and non-Pt oxygen reduction catalysts for PEMFCs. *Appl. Catal., B* **2005**, *56*, 9−35. (b) Katsounaros, I.; Cherevko, S.; Zeradjanin, A. R.; Mayrhofer, K. J. J. Oxygen Electrochemistry as a Cornerstone for Sustainable Energy Conversion. *Angew. Chem., Int. Ed.* **2014**, *53*, 102−121.

(2) For review articles, see: (a) Anson, F. C.; Shi, C.; Steiger, B. Novel Multinuclear Catalysts for the Electroreduction of Dioxygen Directly to Water. *Acc. Chem. Res.* **1997**, *30*, 437−444. (b) Collman, J. P.; Wagenknecht, P. S.; Hutchison, J. E. Molecular Catalysts for Multielectron Redox Reactions of Small Molecules: The "Cofacial Metallodiporphyrin" Approach. *Angew. Chem., Int. Ed.* **1994**, *33*, 1537−1554. (c) Collman, J. P.; Boulatov, R.; Sunderland, C. J.; Fu, L. Functional Analogues of Cytochrome *c* Oxidase, Myoglobin, and Hemoglobin. *Chem. Rev.* **2004**, *104*, 561−588. (d) Rosenthal, J.; Nocera, D. G. Role of Proton-Coupled Electron Transfer in O−O Bond Activation. *Acc. Chem. Res.* **2007**, *40*, 543−553. (e) Savéant, J.-M. Molecular Catalysis of Electrochemical Reactions. Mechanistic Aspects. *Chem. Rev.* **2008**, *108*, 2348−2378.

(3) For other leading references, see: (a) Collman, J. P.; Denisevich, P.; Konai, Y.; Marrocco, M.; Koval, C.; Anson, F. C. Electrode Catalysis of the Four-Electron Reduction of Oxygen to Water by Dicobalt Face-to-Face Porphyrins. *J. Am. Chem. Soc.* **1980**, *102*, 6027−6036. (b) Kadish, K. M.; Frémond, L.; Shen, J.; Chen, P.; Ohkubo, K.; Fukuzumi, S.; El Ojaimi, M.; Gros, C. P.; Barbe, J.-M.; Guilard, R. Catalytic Activity of Biscobalt Porphyrin-Corrole Dyads Toward the Reduction of Dioxygen. *Inorg. Chem.* **2009**, *48*, 2571−2582. (c) Carver, C. T.; Matson, B. D.; Mayer, J. M. Electrocatalytic Oxygen Reduction by Iron Tetraarylporphyrins Bearing Pendant Proton Relays. *J. Am. Chem. Soc.* **2012**, *134*, 5444−5447. (d) Mase, K.; Ohkubo, K.; Fukuzumi, S. Efficient Two-Electron Reduction of Dioxygen to Hydrogen Peroxide with One-Electron Reductants with a Small Overpotential Catalyzed by a Cobalt Chlorin Complex. *J. Am. Chem. Soc.* **2013**, *135*, 2800−2808.

(4) Baran, J. D.; Grönbeck, H.; Hellman, A. Analysis of Porphyrines as Catalysts for Electrochemical Reduction of O_2 and Oxidation of H_2O. *J. Am. Chem. Soc.* **2014**, *136*, 1320−1326.

(5) Dogutan, D. K.; Stoian, S. A.; McGuire, R., Jr.; Schwalbe, M.; Teets, T. S.; Nocera, D. G. Hangman Corroles: Efficient Synthesis and Oxygen Reaction Chemistry. *J. Am. Chem. Soc.* **2011**, *133*, 131−140.

(6) Geiger, T.; Anson, F. C. Homogeneous Catalysis of the Electrochemical Reduction of Dioxygen by a Macrocyclic Cobalt(III) Complex. *J. Am. Chem. Soc.* **1981**, *103*, 7489−7496.

(7) Chan, R. J. H.; Su, Y. O.; Kuwana, T. Electrocatalysis of Oxygen Reduction. 5. Oxygen to Hydrogen Peroxide Conversion by Cobalt(II) Tetrakis(N-methyl-4-pyridyl)porphyrin. *Inorg. Chem.* **1985**, *24*, 3777−3784.

(8) D'Souza, F.; Hsieh, Y.-Y.; Deviprasad, G. R. Electrocatalytic reduction of molecular oxygen using non-planar cobalt tetrakis-(4-sulfonatophenyl)-*β*-octabromoporphyrin. *J. Electroanal. Chem.* **1997**, *426*, 17−21.

(9) For reviews of aerobic oxidation reactions of this type, see: (a) Stahl, S. S. Palladium Oxidase Catalysis: Selective Oxidation of

DOI: 10.1021/acscentsci.5b00163
ACS Cent. Sci. 2015, 1, 234−243

Organic Chemicals by Direct Dioxygen-Coupled Turnover. *Angew. Chem., Int. Ed.* **2004**, *43*, 3400−3420. (b) Piera, J.; Bäckvall, J.-E. Catalytic Oxidation of Organic Substrates by Molecular Oxygen and Hydrogen Peroxide by Multistep Electron Transfer—A Biomimetic Approach. *Angew. Chem., Int. Ed.* **2008**, *47*, 3506−3523.

(10) See, for example: (a) Chaudhuri, P.; Hess, M.; Flörke, U.; Wieghardt, K. From Structural Models of Galactose Oxidase to Homogeneous Catalysis: Efficient Aerobic Oxidation of Alcohols. *Angew. Chem., Int. Ed.* **1998**, *37*, 2217−2220. (b) Bianchi, D.; Bortolo, R.; D'Aloisio, R.; Ricci, M. Biphasic Synthesis of Hydrogen Peroxide from Carbon Monoxide, Water, and Oxygen Catalyzed by Palladium Complexes with Bidentate Nitrogen Ligands. *Angew. Chem., Int. Ed.* **1999**, *38*, 706−708.

(11) See, for example: (a) Steinhoff, B. A.; Fix, S. R.; Stahl, S. S. Mechanistic Study of Alcohol Oxidation by the $Pd(OAc)_2/O_2$/DMSO Catalyst System and Implications for the Development of Improved Aerobic Oxidation Catalysts. *J. Am. Chem. Soc.* **2002**, *124*, 766−767. (b) Hoover, J. M.; Ryland, B. L.; Stahl, S. S. Mechanism of Copper(I)/TEMPO-Catalyzed Aerobic Alcohol Oxidation. *J. Am. Chem. Soc.* **2013**, *135*, 2357−2367.

(12) Pourbaix, M.; de Zoubov, N. In *Atlas D'Équilibres Électrochimiques*; Pourbaix, M., Ed.; Gauthier-Villars: Paris, 1963; pp 97−105.

(13) Derived from data in (a) Wagman, D. D.; Evans, W. H.; Parker, V. B.; Schumm, R. H.; Halow, I.; Bailey, S. M.; Churney, K. L.; Nuttall, R. L. The NBS tables of chemical thermodynamic properties. Selected values for inorganic and C_1 and C_2 organic substances in SI units. *J. Phys. Chem. Ref. Data* **1982**, *11*, Suppl. 2. (b) Chase, M. W., Jr. NIST-JANAF Thermochemical Tables, Fourth Edition Part I, Al-Co. *J. Phys. Chem. Ref. Data*, **1998**, Monograph 9.

(14) See also: Wardman, P. Reduction Potentials of One Electron Couples Involving Free Radicals in Aqueous Solution. *J. Phys. Chem. Ref. Data* **1989**, *18*, 1637−1755.

(15) Ford, P. C.; Wink, D. A.; Stanbury, D. M. Autoxidation kinetics of aqueous nitric oxide. *FEBS Lett.* **1993**, *326*, 1−3.

(16) Rosca, V.; Duca, M.; de Groot, M. T.; Koper, M. T. M. Nitrogen Cycle Electrocatalysis. *Chem. Rev.* **2009**, *109*, 2209−2244.

(17) For an exception, see: Banks, C. E.; Goodwin, A.; Heald, C. G. R.; Compton, R. G. Exploration of gas sensing possibilities with edge plane pyrolytic graphite electrodes: nitrogen dioxide detection. *Analyst* **2005**, *130*, 280−282.

(18) (a) Kummer, J. T.; Oei, D.-G. A chemically regenerative redox fuel cell. II. *J. Appl. Electrochem.* **1985**, *15*, 619−629. (b) Bergens, S. H.; Gorman, C. B.; Palmore, G. T. R; Whitesides, G. M. A Redox Fuel Cell That Operates with Methane as Fuel at 120 °C. *Science* **1994**, *265*, 1418−1420.

(19) See, for example: Wu, C.-H.; Liao, H.-Y.; Hsueh, K.-L.; Hung, J.-S. Study of the Kinetics of Vanadium Redox Reaction by Rotating Disk Electrode. *ECS Trans.* **2011**, *35* (32), 11−22.

(20) For reviews, see: (a) Wertz, S.; Studer, A. Nitroxide-catalyzed transition-metal-free aerobic oxidation processes. *Green Chem.* **2013**, *15*, 3116−3134. (b) Cao, Q.; Dornan, L. M.; Rogan, L.; Hughes, N. L.; Muldoon, M. J. Aerobic oxidation catalysis with stable radicals. *Chem. Commun.* **2014**, *50*, 4524−4543.

(21) For relevant precedents, see: (a) Liu, R.; Liang, X.; Dong, C.; Hu, X. Transition-Metal-Free: A Highly Efficient Catalytic Aerobic Alcohol Oxidation Process. *J. Am. Chem. Soc.* **2004**, *126*, 4112−4113. (b) Liu, R.; Dong, C.; Liang, X.; Wang, X.; Hu, X. Highly Efficient Catalytic Aerobic Oxidations of Benzylic Alcohols in Water. *J. Org. Chem.* **2005**, *70*, 729−731. (c) Shibuya, M.; Osada, Y.; Sasano, Y.; Tomizawa, M.; Iwabuchi, Y. Highly Efficient, Organocatalytic Aerobic Alcohol Oxidation. *J. Am. Chem. Soc.* **2011**, *133*, 6497−6500. (d) Rahimi, A.; Azarpira, A.; Kim, H.; Ralph, J.; Stahl, S. S. Chemoselective Metal-Free Aerobic Alcohol Oxidation in Lignin. *J. Am. Chem. Soc.* **2013**, *135*, 6415−6418. (e) Lauber, M. B.; Stahl, S. S. Efficient Aerobic Oxidation of Secondary Alcohols at Ambient Temperature with an ABNO/NO_x Catalyst System. *ACS Catal.* **2013**, *3*, 2612−2616. (f) Ionita, P. A mechanistic glimpse into the oxidation of alcohols using TEMPO/NO_x catalytic systems: towards a greener bifunctional catalyst. *RSC Adv.* **2013**, *3*, 21218−21221. (g) Holan, M.; Jahn, U. Anaerobic Nitroxide-Catalyzed Oxidation of Alcohols Using the $NO^+/NO^\bullet$ Redox Pair. *Org. Lett.* **2014**, *16*, 58−61. (h) Shibuya, M.; Nagasawa, S.; Osada, Y.; Iwabuchi, Y. Mechanistic Insight into Aerobic Alcohol Oxidation Using NO_x−Nitroxide Catalysis Based on Catalyst Structure−Activity Relationships. *J. Org. Chem.* **2014**, *79*, 10256−10268.

(22) (a) Janiszewska, A. M.; Grzeszczuk, M. Mechanistic − Kinetic Scheme of Oxidation/Reduction of TEMPO Involving Hydrogen Bonded Dimer. RDE Probe for Availability of Protons in Reaction Environment. *Electroanalysis* **2004**, *16*, 1673−1681. (b) Israeli, A.; Patt, M.; Oron, M.; Samuni, A.; Kohen, R.; Goldstein, S. Kinetics and mechanism of the comproportionation reaction between oxoammonium cation and hydroxylamine derived from cyclic nitroxides. *Free Radical Biol. Med.* **2005**, *38*, 317−324. (c) Bobbitt, J. M.; Merbouh, N. Preparation of 4-acetylamino-2, 2, 6, 6- tetramethylpiperidine-1-oxoammonium tetrafluoroborate, and the oxidation of geraniol to geranial (2,6-Octadienal, 3,7-dimethyl-, (2E)-). *Org. Synth.* **2005**, *82*, 80−86.

(23) TEMPOH solutions were prepared by neutralization of $[TEMPOH_2]BF_4$ with $NaCF_3CO_2$. The UV-visible spectrum in Figure 1A is background corrected for excess base. The synthesis of $[TEMPOH_2]BF_4$ is described in the Supporting Information, and the $TEMPO^+BF_4^-$ was synthesized by the protocol of Bobbitt, J. M.; Guttermuth, M. C. F.; Ma, Z.; Tang, H. Organic Nitrosonium Salts. II. Stability Studies and Oxidations of Some Indole Derivatives. *Heterocycles* **1990**, *30*, 1131−1140.

(24) Fitting was performed using a spreadsheet implementation of the method in Bijlsma, S.; Boelens, H. F. M.; Smilde, A. K. Determination of Rate Constants in Second-Order Kinetics Using UV-Visible Spectroscopy. *Appl. Spectrosc.* **2001**, *55*, 77−83.

(25) Riordan, E.; Minogue, N.; Healy, D.; O'Driscoll, P.; Sodeau, J. R. Spectroscopic and Optimization Modeling Study of Nitrous Acid in Aqueous Solution. *J. Phys. Chem. A* **2005**, *109*, 779−786.

(26) Comparison to spectra in the literature rule out the presence of detectable amounts of dissolved NO_2 or N_2O_3 under the reaction conditions (a) Shaw, A. W.; Vosper, A. J. Dinitrogen Trioxide. Part XI. The Electronic Spectrum of Dinitrogen Trioxide. *J. Chem. Soc., Dalton Trans.* **1972**, 961−964. (b) Mérienne, M. F.; Jenouvrier, A.; Coquart, B. The NO_2 Absorption Spectrum. I: Absorption Cross-Sections at Ambient Temperature in the 300−500 nm Region. *J. Atmos. Chem.* **1995**, *20*, 281−297. (c) Coquart, B.; Jenouvrier, A.; Mérienne, M. F. The NO_2 Absorption Spectrum. II. Absorption Cross-Sections at Low Temperatures in the 400−500 nm Region. *J. Atmos. Chem.* **1995**, *21*, 251−261. (d) Mérienne, M. F.; Jenouvrier, A.; Coquart, B.; Lux, J. P. The NO_2 Absorption Spectrum. IV: The 200−400 nm Region at 220 K. *J. Atmos. Chem.* **1997**, *27*, 219−232.

(27) N_2O_4 has a weak absorption with a peak at 340 nm that may be obscured by the HNO_2 peaks. cf. ref 26d.

(28) Nonaqueous potentials and currents are given relative to ferrocene with the IUPAC sign convention: (a) Bates, R. G.; et al. Recommendations for Sign Conventions and Plotting of Electrochemical Data. *Pure Appl. Chem.* **1976**, *45*, 131−134. (b) Gritzner, G.; Kůta, J. Recommendations on Reporting Electrode Potentials in Nonaqueous Solvents. *Pure Appl. Chem.* **1982**, *54*, 1527−1532.

(29) Constant-potential electrolysis of a trifluoroacetic acid/acetonitrile solution of TEMPO/$NaNO_2$ at 0.20 V, under anaerobic conditions similar to those in Figure 2, leads to total charge passage consistent with bulk reduction of nitrite to NO. In a representative experiment, 0.83 mmol of $NaNO_2$ was added after a pre-electrolysis period during which the TEMPO was reduced until no current continued to flow. During the electrolysis, TEMPO catalyzed the reduction of nitrite (which is in the NO^+ oxidation state), and 91.9 Coulombs were passed. This amount of charge corresponds to 0.95 mmol of electrons, or 1.1 e^- per nitrite, suggesting that nitrite is reduced to NO. An additional implication of these results is that oxygen is necessary for sustained current; see Figure S2 and associated discussion.

(30) The reversible NO/NO^+ couple is observed at a similar potential in rigorously dry CH_3CN. See: Lee, K. Y.; Kuchynka, D. J.; Kochi, J. K. Redox Equilibria of the Nitrosonium Cation and of Its Nonbonded Complexes. *Inorg. Chem.* **1990**, *29*, 4196−4204.

DOI: 10.1021/acscentsci.5b00163
ACS Cent. Sci. 2015, 1, 234−243

(31) The observed TOF may be constrained by transport of the oxoammonium to the electrode from the stirred bulk of the solution. For calculations giving approximate current densities in the absence of mass transport limitations, see Section 9 of the Supporting Information.
(32) A rapid decay in the current is observed at longer time periods (Figure S3), which is tentatively attributed to complete loss of active NO_x species to chemical decomposition pathways. Control experiments in which water was added during the reaction suggest that water formed from O_2 reduction contributes to NO_x decomposition. The NO_x decomposition pathway is not well understood, although considerable recovery of catalytic activity can be achieved by adding trifluoroacetic anhydride (as a dehydrating agent) together with more $NaNO_2$ to the solution (Figure S5). For further discussion of water-promoted decomposition of NO_x, see ref 21h, and the following: Aellig, C.; Girard, C.; Hermans, I. Aerobic Alcohol Oxidations Mediated by Nitric Acid. *Angew. Chem., Int. Ed.* **2011**, *50*, 12355−12360.
(33) See Figures S6-S11. At equilibrium, $[ACT^+]/[ACT] \approx 0.8$ and $[3\text{-}CARP^+]/[3\text{-}CARP] \approx 0.3$.
(34) UV−vis studies of ABNO disproportionation show that the reaction is >100-fold faster than with TEMPO and achieves nearly complete disproportionation ($[ABNO^+]/[ABNO] > 100$ at equilibrium). See Figure S10 and associated text for details.
(35) For a review on catalytic electrochemical reactions using mediators, see: Francke, R.; Little, R. D. Redox catalysis in organic electrosynthesis: basic principles and recent developments. *Chem. Soc. Rev.* **2014**, *43*, 2492−2521.
(36) (a) Goldstein, S.; Samuni, A.; Russo, A. Reaction of Cyclic Nitroxides with Nitrogen Dioxide: The Intermediacy of the Oxoammonium Cations. *J. Am. Chem. Soc.* **2003**, *125*, 8364−8370. (b) Goldstein, S.; Samuni, A.; Merenyi, G. Reactions of Nitric Oxide, Peroxynitrite, and Carbonate Radicals with Nitroxides and Their Corresponding Oxoammonium Cations. *Chem. Res. Toxicol.* **2004**, *17*, 250−257. (c) Samuni, Y.; Samuni, U.; Goldstein, S. The use of cyclic nitroxide radicals as HNO scavengers. *J. Inorg. Biochem.* **2013**, *118*, 155−161.
(37) Electron-transfer rates at the electrode can be approximated from the self-exchange rates via Marcus theory. See Section 9 of the Supporting Information and the following: (a) Marcus, R. A. On the Theory of Oxidation-Reduction Reactions Involving Electron Transfer. V. Comparison and Properties of Electrochemical and Chemical Rate Constants. *J. Phys. Chem.* **1963**, *67*, 853−857. (b) Marcus, R. A. On the Theory of Electron-Transfer Reactions. VI. Unified Treatment for Homogeneous and Electrode Reactions. *J. Chem. Phys.* **1965**, *43*, 679−701.
(38) (a) Wu, L.; Guo, X.; Wang, J.; Guo, Q.; Liu, Z.; Liu, Y. Kinetic studies on the single electron transfer reaction between 2,2,6,6-tetramethylpiperidine oxoammonium ions and phenothiazines: the application of Marcus theory. *Sci. China Ser. B* **1999**, *42*, 138−144. (b) Grampp, G.; Rasmussen, K. Solvent dynamical effects on the electron self-exchange rate of the TEMPO•/TEMPO+ couple (TEMPO = 2,2,6,6-tetramethyl-1-piperidinyloxy radical) Part I. ESR-linebroadening measurements at T = 298 K. *Phys. Chem. Chem. Phys.* **2002**, *4*, 5546−5549.
(39) Awad, H. H.; Stanbury, D. M. Electron Transfer between Azide and Chlorine Dioxide: The Effect of Solvent Barrier Nonadditivity. *J. Am. Chem. Soc.* **1993**, *115*, 3636−3642.
(40) (a) Grätzel, M.; Henglein, A.; Lilie, J.; Beck, G. Pulsradiolytische Untersuchung einiger Elementarprozesse der Oxydation und Reduktion des Nitritions. *Ber. Bunsen-Ges. Phys. Chem.* **1969**, *73*, 646−653. (b) Grätzel, M.; Taniguchi, S.; Henglein, A. Pulsradiolytische Untersuchung der NO-Oxydation und des Gleichgewichts $N_2O_3 \rightleftarrows NO + NO_2$ in wäßriger Lösung. *Ber. Bunsen-Ges. Phys. Chem.* **1970**, *74*, 488−492. (c) Rayson, M. S.; Mackie, J. C.; Kennedy, E. M.; Dlugogorski, B. Z. Accurate Rate Constants for Decomposition of Aqueous Nitrous Acid. *Inorg. Chem.* **2012**, *51*, 2178−2185.
(41) By decreasing the steady-state NO_2 concentration, the equilibrium between NO_2 and nitric acid, which is second-order in $[NO_2]$, is shifted away from HNO_3. Factors limiting the overall catalyst lifetime in this system are not fully understood and may involve a complex interaction between diverse NO_x species, the amount of acid present, and water (cf. Figures S3−S5 and ref 32).
(42) Stamler, J. S.; Singel, D. J.; Loscalzo, J. Biochemistry of Nitric Oxide and Its Redox-Activated Forms. *Science* **1992**, *258*, 1898−1902.
(43) The rich complexity of NO_x chemistry can be seen in work towards its employment as a rocket propellant, which motivated much of the work to obtain the thermodynamic data cited in ref 13. For an introduction, see: Clark, J. D. *IGNITION! An Informal History of Liquid Rocket Propellants*; Rutgers University Press: New Brunswick, NJ, 1972; pp 47−65.
(44) (a) Collman, J. P.; Marrocco, M.; Denisevich, P.; Koval, C.; Anson, F. C. Potent Catalysis of the Electroreduction of Oxygen to Water by Dicobalt Porphyrin Dimers Adsorbed on Graphite Electrodes. *J. Electroanal. Chem.* **1979**, *101*, 117−122. (b) Durand, R. R., Jr.; Bencosme, C. S.; Collman, J. P.; Anson, F. C. Mechanistic Aspects of the Catalytic Reduction of Dioxygen by Cofacial Metalloporphyrins. *J. Am. Chem. Soc.* **1983**, *105*, 2710−2718. (c) Chang, C. K.; Liu, H. Y.; Abdalmuhdi, I. Electroreduction of Oxygen by Pillared Cobalt Cofacial Diporphyrin Catalysts. *J. Am. Chem. Soc.* **1984**, *106*, 2725−2726. (d) Fukuzumi, S.; Mochizuki, S.; Tanaka, T. Efficient Reduction of Dioxygen with Ferrocene Derivatives, Catalyzed by Metalloporphyrins in the Presence of Perchloric Acid. *Inorg. Chem.* **1989**, *28*, 2459−2465. (e) Chang, C. J.; Deng, Y.; Shi, C.; Chang, C. K.; Anson, F. C.; Nocera, D. G. Electrocatalytic four-electron reduction of oxygen to water by a highly flexible cofacial cobalt bisporphyrin. *Chem. Commun.* **2000**, 1355−1356. (f) McCrory, C. C. L.; Devadoss, A.; Ottenwaelder, X.; Lowe, R. D.; Stack, T. D. P.; Chidsey, C. E. D. Electrocatalytic O_2 Reduction by Covalently Immobilized Mononuclear Copper(I) Complexes: Evidence for a Binuclear Cu_2O_2 Intermediate. *J. Am. Chem. Soc.* **2011**, *133*, 3696−3699. (g) Tse, E. C. M.; Schilter, D.; Gray, D. L.; Rauchfuss, T. B.; Gewirth, A. A. Multicopper Models for the Laccase Active Site: Effect of Nuclearity on Electrocatalytic Oxygen Reduction. *Inorg. Chem.* **2014**, *53*, 8505−8516.
(45) (a) Carter, M. J.; Rillema, D. P.; Basolo, F. Oxygen Carrier and Redox Properties of Some Neutral Cobalt Chelates. Axial and In-Plane Ligand Effects. *J. Am. Chem. Soc.* **1974**, *96*, 392−400. (b) Walker, F. A.; Beroiz, D.; Kadish, K. M. Electronic Effects in Transition Metal Porphyrins. 2. The Sensitivity of Redox and Ligand Addition Reactions in Para-Substituted Tetraphenylporphyrin Complexes of Cobalt(II). *J. Am. Chem. Soc.* **1976**, *98*, 3484−3489.
(46) Nonporphyrin Cu complexes have been developed that are competent ORR catalysts and are not constrained to a $M^{III/II}$ potential. However, they escape the limitations of the $Co^{III/II}$ potential by trading it for the limitations of the $Cu^{II/I}$ potential. For example, see ref 44f.
(47) Kadish, K. M.; Frémond, L.; Ou, Z.; Shao, J.; Shi, C.; Anson, F. C.; Burdet, F.; Gros, C. P.; Barbe, J.-M.; Guilard, R. Cobalt(III) Corroles as Electrocatalysts for the Reduction of Dioxygen: Reactivity of a Monocorrole, Biscorroles, and Porphyrin-Corrole Dyads. *J. Am. Chem. Soc.* **2005**, *127*, 5625−5631.
(48) Protons play a central role in the ORR reaction, and uncertainty in the proton activity is directly related to uncertainty in the thermodynamic potential. Because the proton activity in nonaqueous media is difficult to measure exactly, the most direct way to compare the performance of O_2 reduction catalysts is to study them under identical conditions. Then, the difference in overpotential can be unambiguously determined even if the overpotential itself remains only approximately known.
(49) In order to make this comparison, the $Co^{III/II}$ potential for CoTPP was determined by CV under conditions identical to the nitroxyl/NO_x-catalyzed ORR experiments described here (viz., 9:1 CH_3CN:CF_3CO_2H) (cf. Figures 4 and S13). The observed potential (−0.05 V vs Fc/Fc^+) is within 20 mV of a value obtained previously for CoTPP in acetonitrile containing 10 mM $HClO_4$ (see ref 44d), indicating that this potential is insensitive to the proton source.
(50) Roberts, J. A. S.; Bullock, R. M. Direct Determination of Equilibrium Potentials for Hydrogen Oxidation/Production by Open Circuit Potential Measurements in Acetonitrile. *Inorg. Chem.* **2013**, *52*, 3823−3835.

DOI: 10.1021/acscentsci.5b00163
ACS Cent. Sci. 2015, 1, 234−243

(51) See also: Fourmond, V.; Jacques, P.-A.; Fontecave, M.; Artero, V. H_2 Evolution and Molecular Electrocatalysts: Determination of Overpotentials and Effect of Homoconjugation. *Inorg. Chem.* **2010**, *49*, 10338−10347.
(52) Compare the potentials in Table 1 (ca. 1 V vs NHE) with those of metal macrocycles in refs 3a and 44b (ca. 0.5 V vs NHE).
(53) (a) Shen, Z.; Dai, J.; Xiong, J.; He, X.; Mo, W.; Hu, B.; Sun, N.; Hu, X. 2,3-Dichloro-5,6-dicyano-1,4-benzoquinone (DDQ)/tert-Butyl Nitrite/Oxygen: A Versatile Catalytic Oxidation System. *Adv. Synth. Catal.* **2011**, *353*, 3031−3038. (b) Wang, L.; Li, J.; Yang, H.; Lv, Y.; Gao, S. Selective Oxidation of Unsaturated Alcohols Catalyzed by Sodium Nitrite and 2,3-Dichloro-5,6-dicyano-1,4-benzoquinone with Molecular Oxygen under Mild Conditions. *J. Org. Chem.* **2012**, *77*, 790−794. (c) Shen, Z.; Sheng, L.; Zhang, X.; Mo, W.; Hu, B.; Sun, N.; Hu, X. Aerobic oxidative deprotection of benzyl-type ethers under atmospheric pressure catalyzed by 2,3-dichloro-5,6-dicyano-1,4-benzoquinone (DDQ)/tert-butyl nitrite. *Tetrahedron Lett.* **2013**, *54*, 1579−1583. (d) Walsh, K.; Sneddon, H. F.; Moody, C. J. Sustainable, mild and efficient p-methoxybenzyl ether deprotections utilizing catalytic DDQ. *Tetrahedron* **2014**, *70*, 7380−7387. (e) Cheng, D.; Yuan, K.; Xu, X.; Yan, J. The oxidative coupling of benzylic compounds catalyzed by 2,3-dichloro-5,6-dicyano-benzoquinone and sodium nitrite using molecular oxygen as a co-oxidant. *Tetrahedron Lett.* **2015**, *56*, 1641−1644. (f) Lancefield, C. S.; Ojo, O. S.; Tran, F.; Westwood, N. J. Isolation of Functionalized Phenolic Monomers through Selective Oxidation and C-O Bond Cleavage of the *β*-O-4 Linkages in Lignin. *Angew. Chem. . Int. Ed.* **2015**, *54*, 258−262.
(54) (a) Muñiz, K. High-Oxidation-State Palladium Catalysis: New Reactivity for Organic Synthesis. *Angew. Chem., Int. Ed.* **2009**, *48*, 9412−9423. (b) Lyons, T. W.; Sanford, M. S. Palladium-Catalyzed Ligand-Directed C−H Functionalization Reactions. *Chem. Rev.* **2010**, *110*, 1147−1169. (c) Powers, D. C.; Ritter, T. Bimetallic Redox Synergy in Oxidative Palladium Catalysis. *Acc. Chem. Res.* **2012**, *45*, 840−850.
(55) (a) Muzart, J. Molecular Oxygen To Regenerate Pd^{II} Active Species. *Chem.—Asian J.* **2006**, *1*, 508−515. (b) Gligorich, K. M.; Sigman, M. S. Recent advancements and challenges of palladium^{II}-catalyzed oxidation reactions with molecular oxygen as the sole oxidant. *Chem. Commun.* **2009**, 3854−3867.
(56) For leading references, see: (a) Khusnutdinova, J. R.; Rath, N. P.; Mirica, L. M. The Aerobic Oxidation of a Pd(II) Dimethyl Complex Leads to Selective Ethane Elimination from a Pd(III) Intermediate. *J. Am. Chem. Soc.* **2012**, *134*, 2414−2422. (b) Qu, F.; Khusnutdinova, J. R.; Rath, N. P.; Mirica, L. M. Dioxygen activation by an organometallic Pd(II) precursor: formation of a Pd(IV)−OH complex and its C−O bond formation reactivity. *Chem. Commun.* **2014**, *50*, 3036−3039.
(57) (a) An, Z.; Pan, X.; Liu, X.; Han, X.; Bao, X. Combined Redox Couples for Catalytic Oxidation of Methane by Dioxygen at Low Temperatures. *J. Am. Chem. Soc.* **2006**, *128*, 16028−16029. (b) Stowers, K. J.; Kubota, A.; Sanford, M. S. Nitrate as a redox co-catalyst for the aerobic Pd-catalyzed oxidation of unactivated sp^3-C−H bonds. *Chem. Sci.* **2012**, *3*, 3192−3195. (c) Wickens, Z. K.; Guzmán, P. E.; Grubbs, R. H. Aerobic Palladium-Catalyzed Dioxygenation of Alkenes Enabled by Catalytic Nitrite. *Angew. Chem., Int. Ed.* **2015**, *54*, 236−240. (d) Liang, Y.-F.; Li, X.; Wang, X.; Yan, Y.; Feng, P.; Jiao, N. Aerobic Oxidation of Pd^{II} to Pd^{IV} by Active Radical Reactants: Direct C−H Nitration and Acylation of Arenes via Oxygenation Process with Molecular Oxygen. *ACS Catal.* **2015**, *5*, 1956−1963. (e) Zultanski, S. L.; Stahl, S. S. Palladium-catalyzed aerobic acetoxylation of benzene using NO_x-based redox mediators. *J. Organomet. Chem.* **2015**, DOI: 10.1016/j.jorganchem.2015.03.003.

DOI: 10.1021/acscentsci.5b00163
ACS Cent. Sci. 2015, 1, 234−243